Original Research Article: full paper

(2023), «EUREKA: Physics and Engineering»
Number 1

# GEOTECHNICAL AND THERMAL ANALYSIS AND COMPLEX IMPEDANCE SPECTROSCOPY CHARACTERIZATION OF PURE MOROCCAN BENTONITE MATERIAL FOR CIVIL ENGINEERING APPLICATIONS

***Mohamed Essaleh*** ✉
*Geosciences, Geonvironnement and Civil Engineering Laboratory*[1]
*moh.essaleh@gmail.com*

***Rachid Bouferra***
*Geosciences, Geonvironnement and Civil Engineering Laboratory*[1]

***Imad Kadiri***
*Laboratory of Advanced Materials and Applications*
*Higher School of Technology*
*Km 5, road of Agouray, N6, Meknes, Morocco, 50040*

***Soufiane Belhouideg***
*Research Laboratory of Physics and Engineers Sciences*
*Team of Applied Physics and New Technologies*[2]

***Mohammed Mansori***
*Laboratory of Innovative Materials, Energy and Sustainable Development*[1]

***Abdeltif Bouchehma***
*Research Laboratory of Physics and Engineers Sciences*
*Team of Applied Physics and New Technologies*[2]

***Mohamed Oubani***
*Laboratory of Innovative Materials, Energy and Sustainable Development*[1]

***Mohamed Benjelloun***
*Geosciences, Geonvironnement and Civil Engineering Laboratory*[1]

[1]*Cadi-Ayyad University*
*549 FSTG, B. P., Marrakech, Morocco, 40000*

[2]*Sultan Moulay Slimane University*
*592 FP, Mghila, B.P., Beni Mellal, Morocco, 23000*

✉**Corresponding author**

**Abstract**

Combined modulus and impedance spectra are employed in the present work to explore electrical inhomogeneity and carriers' behaviors in a pure bentonite Moroccan clay based on equivalent circuit. It has been clearly observed that the electrical properties change due to the increase of temperature from 300 °C to 700 °C. The frequency-dependent imaginary modulus $M''$ and imaginary impedance $Z''$ curves has only one peak at each temperature indicating the predominance of the contribution of grains to the total electrical conduction in bentonite. The positions of these peaks move to higher frequencies when the temperature increases in relation with the distribution of relaxation time. Moreover, the activation energy for the conduction process in bentonite is determined from the slope of $\ln(\rho_{dc})$ versus of $1/T$ in the order of 700 meV in good agreement with that obtained from the proposed equivalent circuit. On the other hand, let's present a geotechnical study that show that our material is a swelling clay, very plastic and could be used as a binder. The external stress dependence of the bulk density, Young's module and maximum stress are analysed. The thermal conductivity determined following the device of Lee's disks where two copper disks of thickness of 15 mm and diameter of 30 mm were used.

**Keywords:** clay, compacted bentonite, microstructure, compressive strength, thermal conductivity, electrical conductivity, impedance spectroscopy.

**DOI: 10.21303/2461-4262.2023.002571**

## 1. Introduction

Impedance and modulus formalisms have been established as one of the most informative investigation methods on revealing the inside heterogeneity and carriers' transport in semiconducting disordered materials. Different temperature and frequency spectra display different features, resulting in varied applications for analysis of the data and reveal useful information about the electrical properties of different structures, e.g., grain, grain boundary and electrode/sample contact [1]. In our previous study on $Cu_5In_9Se_{16}$ [2] and $Fe_2O_3$/Kaolinite [3] ceramics, the powerful technique of complex impedance spectroscopy (IS) is described in order to illustrate the electrical characteristics of some representative disordered semiconducting materials in different temperature ranges from –175 °C to +700 °C. Analytical methods using the second derivative of $\ln(-Z'')$ and $\ln(M'')$ and first derivative of the function $Beta = \arctan(-Z''/Z')$ were presented to identify the dominant microscopic contributions to the electrical conduction [2]. In this paper, frequency-domain responses in impedance and modulus are discussed in detail, taking a pure bentonite Moroccan clay ceramics as an example. Remarkable agreement are found between simulated results and measured data. In general, clays are considered as the most interesting materials because of their low cost and their abundance over all continents [2, 3]. Their small size in natural conditions (less than 2 μm) means that these minerals develop large specific surfaces [4]. Bentonite, one member of the clays' family, designates a mineral powder that consists essentially of montmorillonite [5]. In their natural state, most bentonite deposits are heterogeneous, consisting of smectites interbedded with illite and/or kaolinite and other impurities [6]. The technique of impedance spectroscopy has been used to correlate electrical parameters to permeability, diffusivity and/or porosity in sands, cement-based materials and geological materials [7]. To our knowledge, no detailed works were published in literature about impedance measurements related to the pure bentonite in the high temperature regime up to 700 °C. Thus, the goal of this work is to study the influence of the frequency and temperature on the electrical conductivity of pure industrial bentonite by using the useful nondestructive experimental technique of impedance spectroscopy [8–10]. It permits to measure the frequency dependence of the real part, $Z'$ and the imaginary part, $Z''$ of complex impedance $Z^*(Z^* = Z'+jZ''$, where $j^2 = -1$) at a given temperature $T$. For homogeneous materials, the $Z''$ versus $Z'$ diagram (Nyquist diagram) is a half circle that can be modelized by a resistance $R$ mounted in parallel with a capacitance $C$. This capacitance is replaced by the constant phase element (*CPE*) if there is a distribution of relaxation time in the material. The *IS* characterization will permit to identify and understand the dominant conduction mechanisms in bentonite in the considered frequency and temperature ranges. For this study, the temperature varies between 300 °C to 700 °C. Below about 300 °C, the electrical conductivity of samples is very small. The obtained results permit the investigation of the role of the microstructure of the considered material in the transport properties with the analysis of the influence of the heat treatment on the electrical conductivity. Otherwise, thermal conductivity and volumetric or massic heat capacity are undoubtedly the main parameters related to the efficiency with which heat is transported through the clay. The porosity as well as the bulk density have a major influence on the thermal properties in addition to the thermal conductivity and the heat capacity of the considered clay. In this case, it is very important to know the effect of the bulk density on these properties for a possible use in the building sector, for example. Hence, in addition to the electrical characteristics of bentonite, let's present in this work a study of the physico-chemical, geotechnical and thermo-mechanical as well as to provide useful information for any improvement in the performance of this material.

## 2. Materials and methods

In this section, let's present the experimental methods of preparation of our samples in order to characterize them using different techniques. They are, X-ray fluorescence spectrometry (XRF), X-ray diffraction (XRD), scanning electron microscopy (SEM) coupled with X-ray energy

spectrometry (EDX), infrared spectroscopy (IR), thermogravimetric analysis (TGA) and differential thermal analysis (DTA), laser particle size analysis, geotechnical analysis, thermal and mechanical analysis, and finally complex impedance spectroscopy (SIC). Pure commercial powder bentonite clay is used in the present study (**Fig. 1, *a***). The prepared samples in cylindrical forms for electrical, mechanical and thermal measurements are shown in **Fig. 1**. The corresponding values of diameter and thickness are 13/2 mm, 15/30 mm and 30/15 mm, respectively.

For the electrical case, the pure bentonite powder was first dried at a temperature of 105 °C during 48 h. The dried powder was pressed into discs of about 13 mm in diameter and 2 mm in thickness by means of a hydraulic press with pressure of 50 bars during 2 mn followed by the sintering process at 800 °C for 6 h (**Fig. 2**). The active ingredient in bentonite is montmorillonite mineral, which has a special crystal structure and high swelling property. Montmorillonite is an aluminum silicate in laminar structure containing crystal water and varying charged elements (**Fig. 3**) [11–13]. Montmorillonite is composed of an octahedral (or alumina) sheet sandwiched between two tetrahedral (or silica) sheets. The vertices of the tetrahedra merge with the hydroxyls of the octahedral sheet to form the elementary layer of montmorillonite. The elementary layer has a thickness of about (0.95–0.96) nm [11, 14].

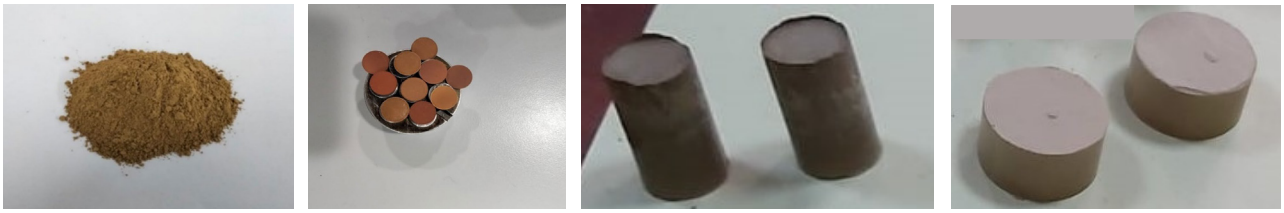

*a* *b* *c* *d*

**Fig. 1.** Samples of bentonite: *a* – powder; *b* – for electrical; *c* – for mechanical; *d* – for thermal conductivity measurements

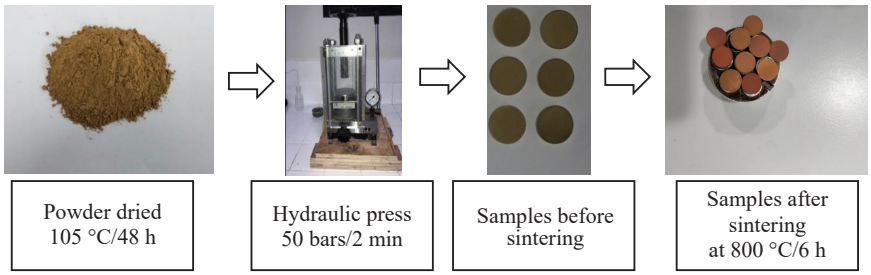


**Fig. 2.** Samples from powder bentonite to pressed sintered cylindrical pellets for electrical measurements

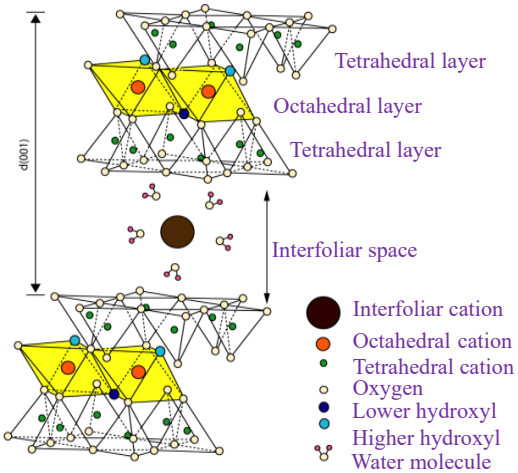


**Fig. 3.** Structure of montmorillonite

### 3. Results and discussion

In this section, let's describe a widely comprehensive experimental characterization of material properties of a pure bentonite Moroccan clay, ranging from microstructure analysis to macroscopic properties relevant for an eventual use in buildings such as thermal conductivity. It can be considered as a good data source for other researchers looking for material data on bentonite. The TGA and DTA analysis (**Fig. 4**) revealed two-stage weight loss. The first one for temperatures lower than 200 °C is mainly due to adhered water molecules in the surface and intercalations bentonite structure. The second one in the temperature range 400–700 °C corresponds to the decomposition of organic counterparts present in the material. The chemical composition is obtained from the XRF spectrometry and is given in **Table 1**.

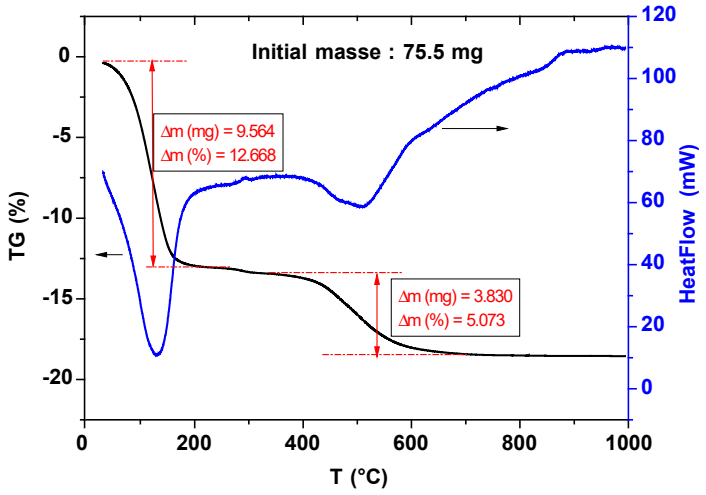


**Fig. 4.** Thermogravimetric analysis (TGA) and differential thermal analysis (DTA) of bentonite

**Table 1**

Chemical characteristics of bentonite by X-ray fluorescence spectrometry

| | $SiO_2$ | $Al_2O_3$ | $Fe_2O_3$ | MgO | CaO | $Na_2O$ | $K_2O$ | $TiO_2$ | $M_nO$ |
|---|---|---|---|---|---|---|---|---|---|
| Chemical composition (%) | 53.50 | 17.22 | 8.97 | 2.60 | 1.37 | 3.4 | 1.2 | 1.32 | 0.03 |

The main chemical composition is $SiO_2$ (53.50 %) mainly from quartz. Concentrations of MgO (2.60 %), CaO (1.37 %) and $Na_2O$ (3.4 %) related to the presence of sodium and dolomite as well as $Al_2O_3$ (17.22 %) related to clay silicates contribute to obtaining good plasticity. The $Al_2O_3/SiO_2$ composition ratio for bentonite is calculated to be 0.32. This value is very close to the theoretical value of 1/3 for montmorillonite indicating that montmorillonite dominates our bentonite. The content of $Na_2O$ is large compared to those of CaO indicating that our bentonite is of sodium type [15, 16]. The crystal structure of bentonite was investigated using the X-ray diffraction technique (XRD, Rigaku, smartLab) with Cu-Kα radiation (the wavelength is $\lambda = 1.5406$ A, $1A = 10^{-10}$ m) in a 2θ range from 5° to 90°, and a scan rate of 5°/min (**Fig. 5, *a*** for the dried powder and **Fig. 5, *b*** for the sintered pellet at 800 °C/6 h).

The analysis of these XRD spectra was made using the X'Pert HighScore software and the dominant phase of montmorillonite with peaks located at $2\theta = 7.21°$, 19.40°, 34.84° and 55.22° is identified in agreement with the XRD data of an Egyptian bentonite of Na-type [16]. Other clay mineral impurities such as quartz and feldspars were also found. The morphological structure of bentonite was determined by the scanning electron microscope (SEM, TESCAN $VEGA_3$) coupled with the chemical microanalysis of energy dispersive X-ray spectrometry (EDX) as shown in **Fig. 6, *a*** for the dried powder and in **Fig. 6, *b*** for the sintered pellet at 800 °C/6 h. The main elements of aluminum (Al), silicon (Si) and oxygen (O) were observed. According to the SEM analysis, the bentonite shows a porous crystalline structure. The corresponding chemical formula

of $Na_{0.49}Ca_{0.30}Al_{1.66}Mg_{0.19}Si_{4.21}O_{11.42}$ and $Na_{0.61}Ca_{0.10}Al_{1.54}Mg_{0.67}Si_{3.90}O_{11.60}$ are deduced for the dried powder and for the sintered pellet.

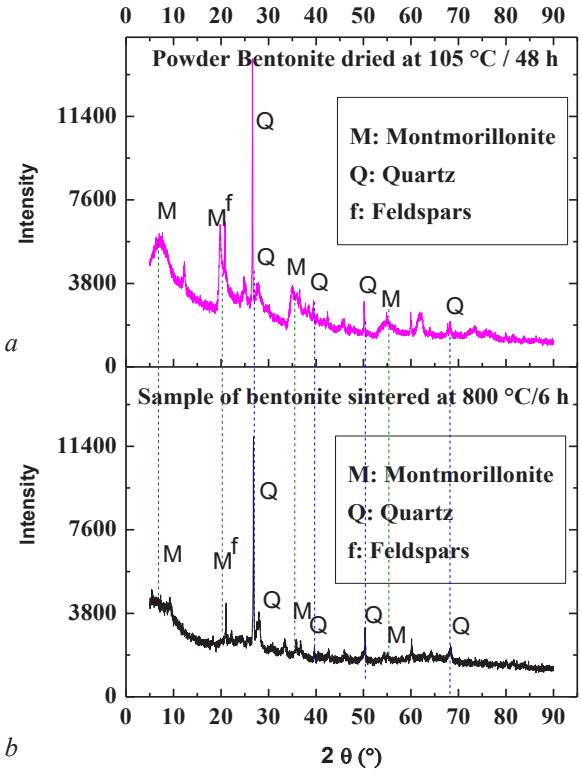


**Fig. 5.** XRD of bentonite: *a* − dried powder at 105 °C/48h; *b* − sintered pellet at 800 °C/6 h

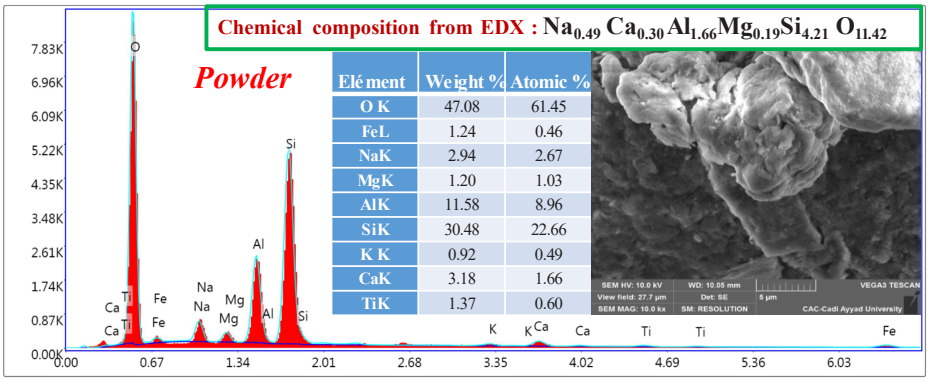


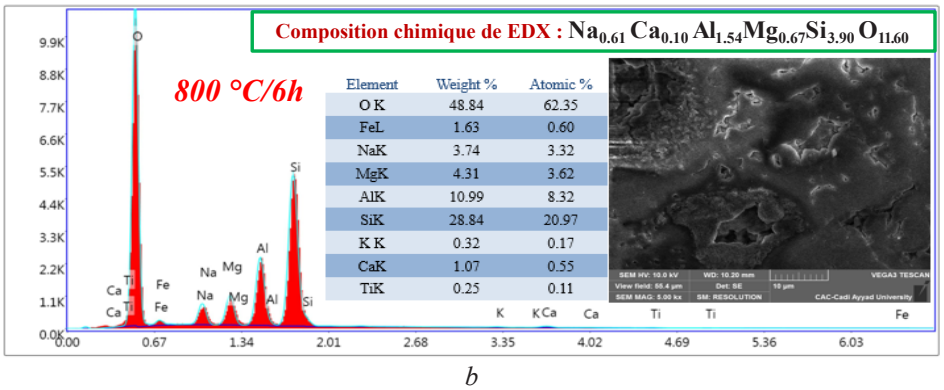


**Fig. 6.** SEM/EDX of bentonite: *a* − dried powder at 105 °C/48h; *b* − sintered pellet at 800 °C/6 h

The characteristic bands of bentonite are shown in **Fig. 7** in agreement with the literature [16, 17].

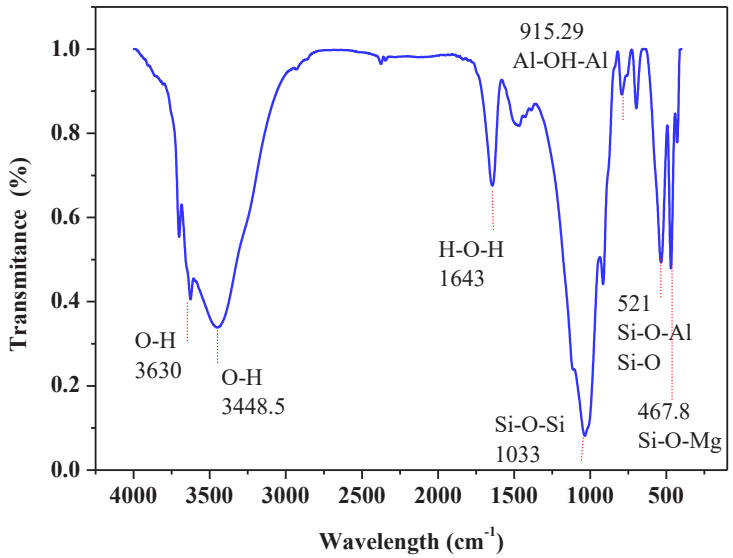


**Fig. 7.** IR spectrum analysis of our bentonite

The particle size curves (**Fig. 8**) shows that our bentonite contains an important quantity of fine particles.

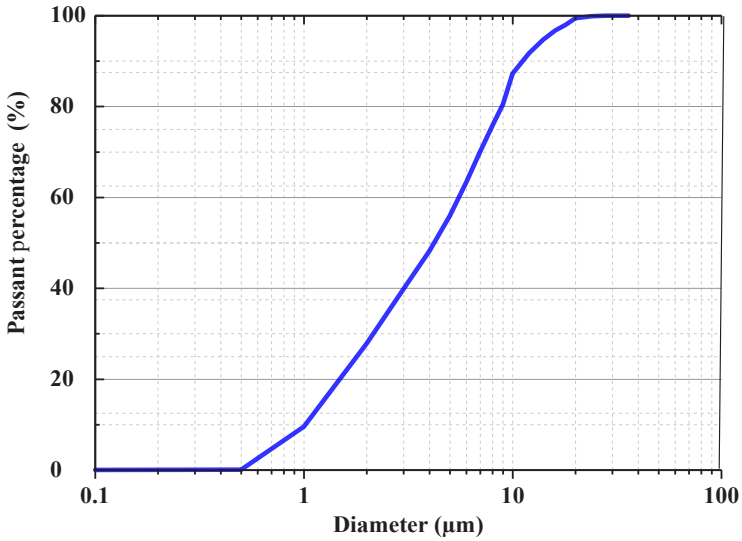


**Fig. 8.** Particle size curve in percentage by fraction of bentonite

According to the distribution of the granular fractions defined by the European standard [NF EN ISO14688-1, 2003], the studied sample consists on a clay fraction (9.56 %), fine silt (48.44 %), medium silt (40.05 %), coarse silt (1.95 %) and 0 % of sand. **Table 2** presents the Atterberg limits, as well as the plasticity, liquidity and consistency index of bentonite. Our bentonite is a very plastic clay ($I_P = 445 > 50$ %) and has a high water content ($W = 246$ %). This is related to the nature of montmorillonite which has a great ability to adsorb water. The methylene blue value (VBS) is determined to be 0.40. According the classification of clays (European standard: NFP 94-068), our bentonite is thus classified as a sandy silty clay, sensitive to water ($0.2 \leq \text{VBS} \leq 1.5$). Our bentonite is classified as a low calcareous material, with the calcium carbonate content of the order of 10.23 % exceeding 10 %. The solid particle density is determined to be around 1.81 g/cm$^3$.

**Table 2**
Geotechnical characteristics of bentonite

| | |
|---|---|
| Liquidity limit $W_L$ en % | 500 |
| Plasticity limit $W_p$ en % | 55 |
| Plasticity index $I_p$ en % | 445 |
| Consistency index $I_c$ en % | 0.57 |
| Liquidity index $I_L$ en % | 0.43 |
| Water content $W$ (%) | 246 |

In **Table 3** and **Fig. 9**, the bulk density, the Young's Module, the maximum stress and the thermal conductivity of bentonite are represented as a function of the compacting intensity from 10 bar to 50 bar. With a density (ρ) varying between 1.843 g/cm$^3$ to 2.118 g/cm$^3$, the thermal conductivity (λ) and the maximum stress ($R_c$) vary between 0.3275 W/mK to 0.4456 W/mK and 10.0 MPa to 20.8 MPa, respectively. The mechanical tests consist in determining the nominal resistance $R_c$ in simple compression of the sample in a cylindrical form (**Fig. 1, *c***) with a speed of 0.5 mm/min until rupture (**Fig. 9, *e***). The thermal conductivity of bentonite, considered as insulator material at room temperature, were determined following the device of Lee's disks (**Fig. 9, *f***) [18–20] where two copper disks (*A*) and (*B*) of thickness of 15 mm and diameter of 30 mm were used. The studied sample is placed between these two disks and the temperatures $T_1$ and $T_2$ at both sides of the sample were measured by two thermocouples placed in each disk (**Fig. 9, *f***).

**Table 3**
Thermal conductivity, Young's module and maximum stress of bentonite

| Compacting intensity (bar) | Bulk density (g/cm$^3$) | Thermal Conductivity (W/m·K) | Young's Module (MPa) | Maximum stress (MPa) |
|---|---|---|---|---|
| 10 | 1,843 | 0,3275 | 272 | 10,0 |
| 30 | 2,031 | 0,3948 | 852 | 14,1 |
| 50 | 2,118 | 0,4456 | 1385 | 20,8 |

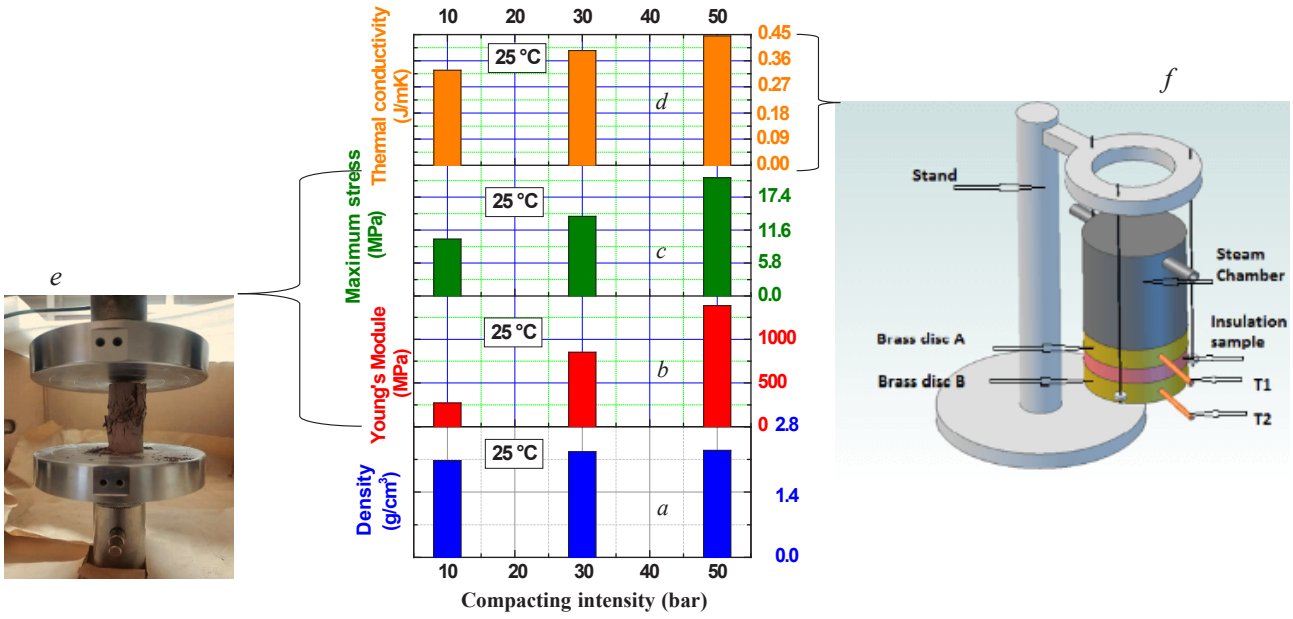


**Fig. 9.** Thermal characteristics of compacted bentonite: *a* – density; *b* – Young's Module; *c* – maximum stress; *d* – thermal conductivity. The experimental setup are also shown: *e* – stress; *f* – thermal conductivity

In this section, let's present some main results of electrical conduction in a representative sample of bentonite sintered at 800 °C/6 h (designated by BC02 for the next). The experimental technique used is complex impedance spectroscopy, which consists in injecting into the sample an alternating signal having an amplitude of the order of 500 mV and a frequency, which varies from 20 Hz to 1 MHz. Given the insulating nature of our material near room temperature, experiments up to 700 °C were conducted. The analysis of the spectra of the complex impedance as well as the electrical modulus allowed to identify the dominant conduction mechanism in bentonite as well as the activation energies for the conduction and for relaxation processes. **Fig. 10, *a*** shows the variations of electrical conductivity (σ) of the sample BC02 as a function of frequency (ω) for different values of temperature between 300 °C and 700 °C, the range where the material starts to conduct electricity. σ increases with ω but also with T indicating the semi-conducting behavior of the material. The experimental curves of $\sigma = \sigma(\omega,T)$ are usually fitted by the universal Jonscher's equation $\sigma(\omega,T) = \sigma_{dc} + A\omega^s$ [10] by considering $\sigma_{dc}$, $A$ and the exponent $s$ as adjusTable parameters. At low frequencies below around 10 kHz (**Fig. 10, *a***), σ takes its lowest value and remains practically frequency independent ($\sigma \approx \sigma_{dc}$). As shown in Fig. 10, *a*, the corresponding value of $\sigma_{dc}$ varies between $1.8 \cdot 10^{-4}$ $(\Omega m)^{-1}$ at 300 °C to $743 \cdot 10^{-4}$ $(\Omega m)^{-1}$ at 700 °C. By plotting $(\ln(\rho_{dc}) = 1/\sigma_{dc})$ as a function of $1/T$ (**Fig. 10, *b***), the activation energy for the conduction process ($E_{cond}$) in bentonite is determined from the slope in the order of 700 meV. Moreover, in the dynamic regime, the electrical modulus $M^*$ is a formalism which is sensitive to the contribution of the «grains» of lower capacity of the order of $10^{-12}$ F [21]. The modulus and the complex impedance ($Z^*$) are given in the expression $(M^*(\omega) = j\omega C_o Z^*(\omega))$ [22, 23] where $C_o$ is the vacuum capacitance $(C_o = \varepsilon_o S/d)$, $S$ and $d$ are the surface and the thickness of the sample.

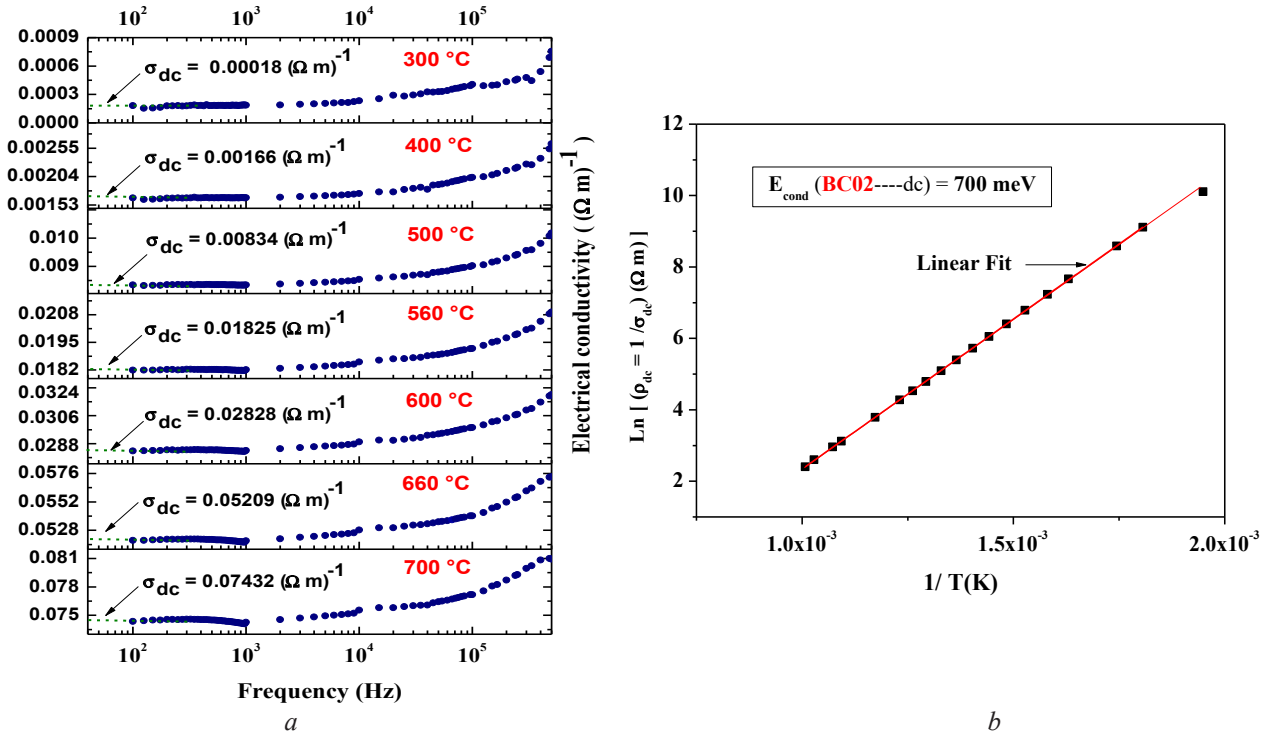


*a* *b*

**Fig. 10**. Electrical characteristics of bentonite:
*a* − Electrical conductivity as a function of frequency for some representative temperatures;
*b* − Temperature dependence of ln ($\rho_{dc} = 1/\sigma_{dc}$)

The frequency dependence of the imaginary parts $Z''$ of $Z^*$ and $M''$ of $M^*$ is given in **Fig. 11** for three representative temperatures of 300 °C, 340 °C and 360 °C. The coincidence of the position of peaks of $Z''$ and $M''$ indicates the predominance of the contribution of grains to the total electrical conduction in bentonite. Also, the positions of these peaks move to higher frequencies

when the temperature increases indicating the distribution of relaxation time in bentonite. It is well known that the Nyquist representation $Z'' = f(Z')$ and $M'' = f(M')$ of the experimental data of $Z^*$ and $M^*$ in the complex plane is the best method to separate and identify the dominant contributions in disordered materials ( grains, grain boundaries and electrodes).

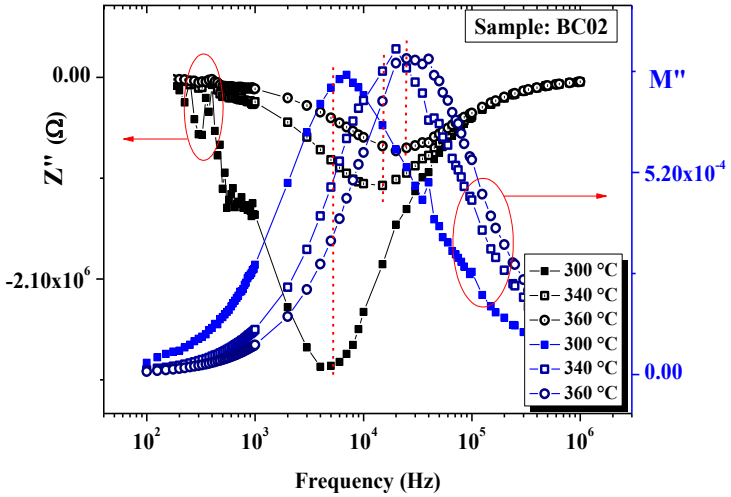


**Fig. 11.** Comparison of the imaginary parts of impedance ($Z''$) and electrical modulus ($M''$) as a function of frequency for some representative temperatures

The observed semi-circles in **Fig. 12, *a*** for $Z^*$ and in **Fig. 12, *b*** for $M^*$ indicate the predominance of one single contribution in BC02, that of the grains. The corresponding resistance $R$ and capacitance $C$ can be estimated from the diameters of these semicircles. In **Fig. 12, *a***, $R$ is of the order of 6.6 MΩ at 300 °C and decreases with increasing temperature in relation to the semi-conductor behavior of our material in this high temperature range. In **Fig. 12, *b***, the capacitance $C$ is deduced in the order of 3.4 pF. The diameter ($C_o/C$) seems to increase when $T$ increases. Thus, $C$ is a decreasing function of $T$ in relation to the dielectric character weakened by the rise in temperature.

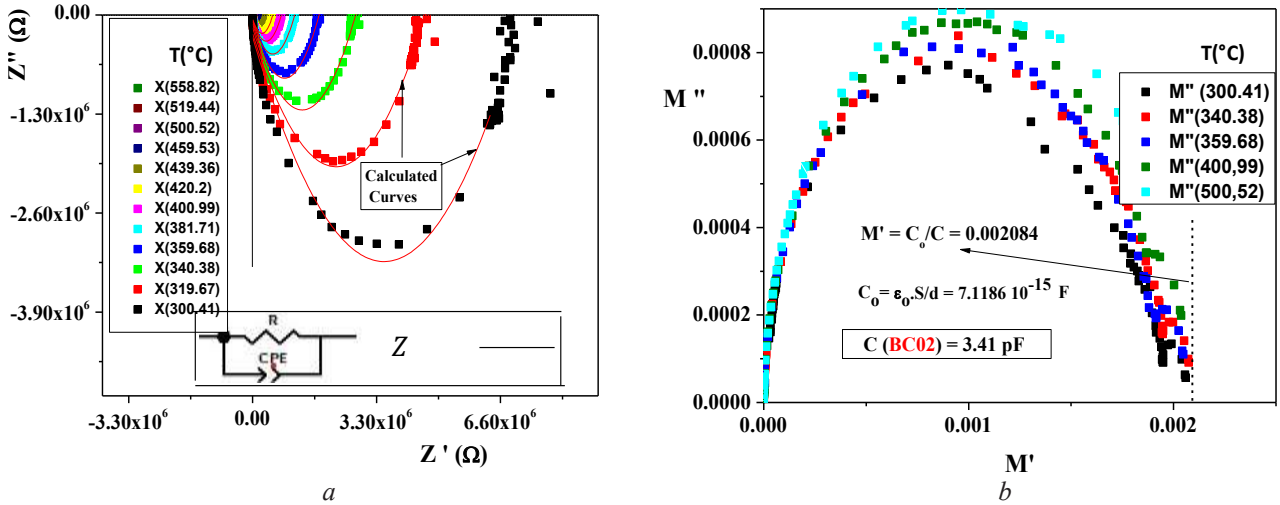


**Fig. 12.** Impedance and Modulus of bentonite for different temperatures:
*a* – $Z'' = f(Z')$; *b* – $M'' = f(M')$

An electric picture can be made for each region of an the electrode-material system (grains, grain boundaries, electrodes, etc.) by considering a resistor and a capacitor mounted in parallel (R//C) [24–26]. In many cases, to take into account the inhomogeneties and also the distribution of the relaxation time in the material, the capacitance $C$ is replaced by a «constant phase

elements» CPE whose impedance is given by $Z_{CPE} = 1/Q(j\omega)^n$. The exponent $n$ measures the degree of distortion of $Z'' = f(Z')$. The value of $n$ is equal to 1 for a pure capacitance. The corresponding calculated curves for $Z^*$ when $R$, $Q$, and $n$ are considered as adjusTable parameters are given in **Fig. 12, *a***.

Their values as well as the deduced relaxation times $\tau = (RQ)^{1/n}$ and capacitance $C = (R^{1-n}Q)^{1/n}$ are listed in **Table 4**. The resistance $R$ varies from 7.05 MΩ at 300 °C to 69.70 kΩ at 560 °C while $C$ varies from 4.63 pF at 300 °C to 3.96 pF at 560 °C. Finally, The activation energies for the conduction and for the relaxation processes can also be estimated from the equivalent electrical circuit for BC02. From the data of $R$ and τ given in **Table 4**, there are plotted $ln(R)$ and $ln(\tau)$ as a function of $1/T$ (**Fig. 13**) that show a perfect linear behaviors. From the corresponding slopes, the activation energies for the conduction and for the relaxations processes $E_{cond}$ and $E_{relax}$ are determined to be $E_{cond}$(BC02_Circ-Eq) = 706 meV and $E_{relax}$(BC02_Circ-Eq) = 728 meV. The value of $E_{cond}$ is in very good agreement with those obtained previously from the analysis of the electrical conductivity. The proposed electrical circuit describes well the electrical conduction in our material.

**Table 4**

Values of the equivalent circuit parameters for BC02 at different temperatures

| *T* (°C) | *R* (Ω) | *Q* | *n* | *C* (F) | *t* (s) |
|---|---|---|---|---|---|
| 300 | $7.05 \cdot 10^{6}$ | $8.56 \cdot 10^{-12}$ | 0.940 | $4.63 \cdot 10^{-12}$ | $3.26 \cdot 10^{-5}$ |
| 320 | $4.16 \cdot 10^{6}$ | $8.49 \cdot 10^{-12}$ | 0.941 | $4.48 \cdot 10^{-12}$ | $1.86 \cdot 10^{-5}$ |
| 360 | $1.67 \cdot 10^{6}$ | $8.32 \cdot 10^{-12}$ | 0.944 | $4.32 \cdot 10^{-12}$ | $7.23 \cdot 10^{-6}$ |
| 380 | $1.09 \cdot 10^{6}$ | $8.81 \cdot 10^{-12}$ | 0.940 | $4.23 \cdot 10^{-12}$ | $4.61 \cdot 10^{-6}$ |
| 400 | 745900 | $9.05 \cdot 10^{-12}$ | 0.938 | $4.17 \cdot 10^{-12}$ | $3.11 \cdot 10^{-6}$ |
| 420 | 524010 | $9.58 \cdot 10^{-12}$ | 0.935 | $4.15 \cdot 10^{-12}$ | $2.17 \cdot 10^{-6}$ |
| 440 | 368160 | $1.01 \cdot 10^{-11}$ | 0.933 | $4.15 \cdot 10^{-12}$ | $1.53 \cdot 10^{-6}$ |
| 460 | 272010 | $1.08 \cdot 10^{-11}$ | 0.929 | $4.13 \cdot 10^{-12}$ | $1.12 \cdot 10^{-6}$ |
| 480 | 200710 | $1.17 \cdot 10^{-11}$ | 0.925 | $4.12 \cdot 10^{-12}$ | $8.27 \cdot 10^{-7}$ |
| 500 | 147980 | $1.28 \cdot 10^{-11}$ | 0.919 | $4.04 \cdot 10^{-12}$ | $5.98 \cdot 10^{-7}$ |
| 520 | 114630 | $1.38 \cdot 10^{-11}$ | 0.915 | $4.01 \cdot 10^{-12}$ | $4.60 \cdot 10^{-7}$ |
| 540 | 88579 | $1.56 \cdot 10^{-11}$ | 0.908 | $3.99 \cdot 10^{-12}$ | $3.53 \cdot 10^{-7}$ |
| 560 | 69705 | $1.78 \cdot 10^{-11}$ | 0.900 | $3.96 \cdot 10^{-12}$ | $2.76 \cdot 10^{-7}$ |

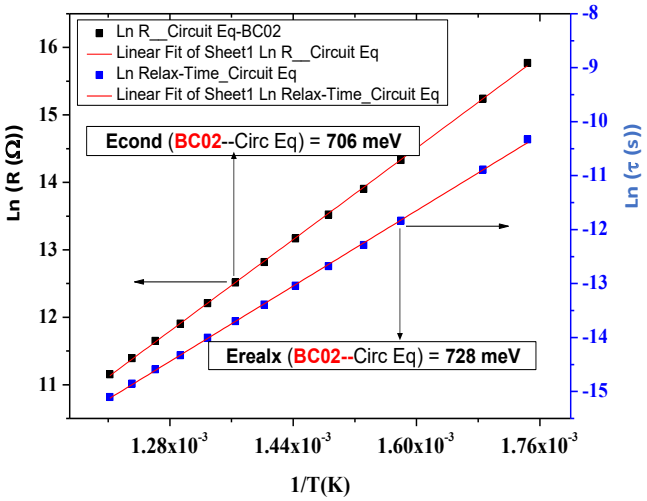


**Fig. 13.** Activation energies for the conduction and for the relaxation processes for the sample BC02

Finally, during a heat treatment of bentonite, this material undergoes physico-chemical transformations which lead to both a modification of its crystalline structure of the different phases and a modification of its microstructure. The development of the ceramic industry requires raw materials with low density of impurities. Indeed the presence of these impurities influences the densification and porosity. These physico-chemical characteristics play an important role in the mechanical, colorimetric and electrical properties. Many experimental and simulation studies have been carried out to understand the microstructure which depends highly on the anisotropy of grain boundary properties such as activation energy, relaxation time, and electrical resistance [27]. The main problem is to identify the predominance of the grain-boundary contribution in the electrical conduction process in a given range of temperature. The complex impedance spectroscopy is the best method to investigate the dielectric relaxation and electrical conduction behaviors of grains and grain boundaries, which are correlated with defect behaviors [28]. In this work, some results are presented using impedance spectroscopy data that allow to identify the predominance of the contribution of grains and/or grain-boundaries to the total electrical conduction in bentonite which is conductive for temperatures higher than 400 °C up to 700 °C. To analyze the dielectric behaviour in bentonite, further studies on the effect of temperature and frequency on the complex permittivity are to be expected.

## 4. Conclusions

The manuscript describes a widely comprehensive characterization of material properties of a pure bentonite Moroccan clay, ranging from microstructure analysis to macroscopic properties relevant for use in buildings such as thermal conductivity. The manuscript provides a solid space of work in the field of materials research for future, more sustainable buildings. It can be considered as a good data source for other researchers looking for material data on bentonite. The data of SEM, EDX, DRX and XRF show that our bentonite is of Na-type with the montmorillonite as the dominant phase. The geotechnical study shows a very plastic silty bentonite, sensitive to water and not very calcareous. For a compacting intensity of 10, 30 and 50 bar, the bulk density ($\rho$) varies between 1.843 g/cm$^3$ to 2.118 g/cm$^3$. The corresponding thermal conductivity ($\lambda$) and the maximum stress ($R_c$) vary between 0.3275 W/mK to 0.4456 W/mK and 10.0 MPa to 20.8 MPa, respectively. The electrical conduction behaviour as well as the activation energies for the conduction and for the relaxation processes are analyzed. The contribution of the grains to the total conduction is identified. The electrical circuit consisting of a resistor connected in parallel with a CPE describes correctly our experimental data.

## Conflict of interest

The authors declare that there is no conflict of interest in relation to this paper, as well as the published research results, including the financial aspects of conducting the research, obtaining and using its results, as well as any non-financial personal relationships.

## Financing

The study was performed without financial support.

## Data availability

Data will be made available on reasonable request.

## References

[1] Huang, Y., Wu, K., Xing, Z., Zhang, C., Hu, X., Guo, P., Zhang, J., Li, J. (2019). Understanding the validity of impedance and modulus spectroscopy on exploring electrical heterogeneity in dielectric ceramics. Journal of Applied Physics, 125 (8), 084103. doi: https://doi.org/10.1063/1.5081842

[2] Essaleh, M., Bouferra, R., Belhouideg, S., Oubani, M., Bouchehma, A., Benjelloun, M. (2022). Electrical characterisation and analysis of dominant contributions in disordered semiconducting systems with an application to the pure bentonite material for civil engineering applications. EUREKA: Physics and Engineering, 6, 164–174. doi: https://doi.org/10.21303/2461-4262.2022.002628

[3] Bouchehma, A., Essaleh, M., Bouferra, R., Belhouideg, S., Benjelloun, M., Sfa, I. (2022). Analysis of frequency dependence of complex impedance and electrical characterization of $Fe_2O_3$/kaolin ceramics for civil engineering applications. EUREKA: Physics and Engineering, 5, 175–183. doi: https://doi.org/10.21303/2461-4262.2022.002312

[4] Dlamini, M. C., Maubane-Nkadimeng, M. S., Moma, J. A. (2021). The use of TiO2/clay heterostructures in the photocatalytic remediation of water containing organic pollutants: A review. Journal of Environmental Chemical Engineering, 9 (6), 106546. doi: https://doi.org/10.1016/j.jece.2021.106546

[5] El-Naggar, M. E., Wassel, A. R., Shoueir, K. (2021). Visible-light driven photocatalytic effectiveness for solid-state synthesis of ZnO/natural clay/TiO2 nanoarchitectures towards complete decolorization of methylene blue from aqueous solution. Environmental Nanotechnology, Monitoring & Management, 15, 100425. doi: https://doi.org/10.1016/j.enmm.2020.100425

[6] Sedaghat, M. E., Rajabpour Booshehri, M., Nazarifar, M. R., Farhadi, F. (2014). Surfactant modified bentonite (CTMAB-bentonite) as a solid heterogeneous catalyst for the rapid synthesis of 3,4-dihydropyrano[c]chromene derivatives. Applied Clay Science, 95, 55–59. doi: https://doi.org/10.1016/j.clay.2014.02.016

[7] Pineda-Piñón, J., Vega-Durán, J. T., Manzano-Ramírez, A., Prokhorov, E., Morales-Sánchez, E., González-Hernández, J. (2008). Mechanical properties and humidity absorption measured through impedance spectroscopy in clays used for adobe production. Applied Clay Science, 40 (1-4), 1–5. doi: https://doi.org/10.1016/j.clay.2007.06.006

[8] Barsoukov, E., Macdonald, J. R. (Eds.) (2005). Impedance Spectroscopy: Theory, Experiment, and Applications. John Wiley & Sons, Inc. doi: https://doi.org/10.1002/0471716243

[9] Elliott, S. R. (1978). Temperature dependence of a.c. conductivity of chalcogenide glasses. Philosophical Magazine B, 37 (5), 553–560. doi: https://doi.org/10.1080/01418637808226448

[10] Jonscher, A. K. (1999). Dielectric relaxation in solids. Journal of Physics D: Applied Physics, 32 (14), R57–R70. doi: https://doi.org/10.1088/0022-3727/32/14/201

[11] Al Kausor, M., Sen Gupta, S., Bhattacharyya, K. G., Chakrabortty, D. (2022). Montmorillonite and modified montmorillonite as adsorbents for removal of water soluble organic dyes: A review on current status of the art. Inorganic Chemistry Communications, 143, 109686. doi: https://doi.org/10.1016/j.inoche.2022.109686

[12] Grim, R. E. (1968). Clay Mineralogy. McGraw-Hill, 596.

[13] Shattar, S. F. A., Zakaria, N. A., Foo, K. Y. (2015). Feasibility of montmorillonite-assisted adsorption process for the effective treatment of organo-pesticides. Desalination and Water Treatment, 57 (29), 13645–13677. doi: https://doi.org/10.1080/19443994.2015.1065439

[14] Do Nascimento, G. M. (2016). Structure of Clays and Polymer-Clay Composites Studied by X-ray Absorption Spectroscopies. Clays, Clay Minerals and Ceramic Materials Based on Clay Minerals. doi: https://doi.org/10.5772/61788

[15] Veblen, D. R. (1990). High-Resolution Transmission Electron Microscopy and Electron Diffraction of Mixed-Layer Illite/Smectite: Experimental Results. Clays and Clay Minerals, 38 (1), 1–13. doi: https://doi.org/10.1346/ccmn.1990.0380101

[16] Abdel Zaher, M. S., Abdel Wahab, S. M., Taha, M. H., Masoud, A. M. (2018). Sorption Characteristics of Iron, Fluoride and Phosphate from Wastewater of Phosphate Fertilizer Plant using Natural Sodium Bentonite. Journal of Membrane Science & Technology, 08 (02). doi: https://doi.org/10.4172/2155-9589.1000186

[17] Kumar, A., Lingfa, P. (2020). Sodium bentonite and kaolin clays: Comparative study on their FT-IR, XRF, and XRD. Materials Today: Proceedings, 22, 737–742. doi: https://doi.org/10.1016/j.matpr.2019.10.037

[18] Hein, A., Müller, N. S., Day, P. M., Kilikoglou, V. (2008). Thermal conductivity of archaeological ceramics: The effect of inclusions, porosity and firing temperature. Thermochimica Acta, 480 (1-2), 35–42. doi: https://doi.org/10.1016/j.tca.2008.09.012

[19] Randazzo, L., Montana, G., Hein, A., Castiglia, A., Rodonò, G., Donato, D. I. (2016). Moisture absorption, thermal conductivity and noise mitigation of clay based plasters: The influence of mineralogical and textural characteristics. Applied Clay Science, 132-133, 498–507. doi: https://doi.org/10.1016/j.clay.2016.07.021

[20] Hein, A., Karatasios, I., Müller, N. S., Kilikoglou, V. (2013). Heat transfer properties of pyrotechnical ceramics used in ancient metallurgy. Thermochimica Acta, 573, 87–94. doi: https://doi.org/10.1016/j.tca.2013.09.024

[21] Irvine, J. T. S., Sinclair, D. C., West, A. R. (1990). Electroceramics: Characterization by Impedance Spectroscopy. Advanced Materials, 2 (3), 132–138. doi: https://doi.org/10.1002/adma.19900020304

[22] Althobaiti, M. G., Belhaj, M., Abdel-Baset, T., Bashal, A. H., Alotaibi, A. A. (2022). Structural, dielectric and electrical properties of new Ni-dopedcopper/bentonite composite. Journal of King Saud University – Science, 34 (5), 102127. doi: https://doi.org/10.1016/j.jksus.2022.102127

[23] Assar, S. T., El-Ghazzawy, E. H., Abosheiasha, H. F. (2022). Study on dielectric properties, electric modulus, and impedance spectroscopy of Ni-Ca ferrite nanoparticles. Materials Chemistry and Physics, 287, 126336. doi: https://doi.org/10.1016/j.matchemphys.2022.126336

[24] El Asri, S., El Hadri, M., Rahim, M. A., Essaleh, L., Ahamdane, H., Hajji, L. et al. (2022). Structural, microstructure and ac impedance spectroscopy investigation of parent and M-doped forsterite $Mg_{1.9}M_{0.1}SiO_4$ (M=Co, Ni and Mn). Physica B: Condensed Matter, 643, 414127. doi: https://doi.org/10.1016/j.physb.2022.414127

[25] Marín, G., Essaleh, L., Amhil, S., Wasim, S. M., Bouferra, R., Zoubir, A. et al. (2020). Electrical impedance spectroscopy characterization of *n* type Cu5In9Se16 semiconductor compound. Physica B: Condensed Matter, 593, 412283. doi: https://doi.org/10.1016/j.physb.2020.412283

[26] Bouchehma, A., Essaleh, L., Marín, G., Essaleh, M., Wasim, S. M., Amhil, S. et al. (2021). Dielectric spectroscopy of *n* type Cu5In9Se16 semiconductor compound. Physica B: Condensed Matter, 622, 413356. doi: https://doi.org/10.1016/j.physb.2021.413356

[27] Olmsted, D. L., Foiles, S. M., Holm, E. A. (2009). Survey of computed grain boundary properties in face-centered cubic metals: I. Grain boundary energy. Acta Materialia, 57 (13), 3694–3703. doi: https://doi.org/10.1016/j.actamat.2009.04.007

[28] Bai, W., Chen, G., Zhu, J. Y., Yang, J., Lin, T., Meng, X. J. et al. (2012). Dielectric responses and scaling behaviors in Aurivillius Bi6Ti3Fe2O18 multiferroic thin films. Applied Physics Letters, 100 (8), 082902. doi: https://doi.org/10.1063/1.3688033

*Received date 21.09.2022*
*Accepted date 20.12.2022*
*Published date 19.01.2023*



***How to cite:*** *Essaleh, M., Bouferra, R., Kadiri, I., Belhouideg, S., Mansori, M., Bouchehma, A., Oubani, M., Benjelloun, M. (2023). Geotechnical and thermal analysis and complex impedance spectroscopy characterization of pure Moroccan bentonite material for civil engineering applications. EUREKA: Physics and Engineering, 1, 152–164. doi: https://doi.org/10.21303/2461-4262.2023.002571*